Chemical Science

ROYAL SOCIETY OF CHEMISTRY

EDGE ARTICLE

View Article Online
View Journal | View Issue

Cite this: *Chem. Sci.*, 2024, **15**, 651

All publication charges for this article have been paid for by the Royal Society of Chemistry

Metal selectivity and translocation mechanism characterization in proteoliposomes of the transmembrane NiCoT transporter NixA from *Helicobacter pylori*†

Jayoh A. Hernandez, [a] Paul S. Micus,[a] Sean Alec Lois Sunga, [a] Luca Mazzei, [b] Stefano Ciurli [b] and Gabriele Meloni *[a]

Essential trace metals play key roles in the survival, replication, and virulence of bacterial pathogens. *Helicobacter pylori* (*H. pylori*), the main bacterial cause of gastric ulcers, requires Ni(II) to colonize and persist in the acidic environment inside the stomach, exploiting the nickel-containing enzyme urease to catalyze the hydrolysis of urea to ammonia and bicarbonate and create a pH-buffered microenvironment. Urease utilizes Ni(II) as a catalytic cofactor for its activity. In ureolytic bacteria, unique transmembrane (TM) transporters evolved to guarantee the selective uptake and efflux of Ni(II) across cellular membranes to meet the cellular requirements. NixA is an essential Ni(II) transporter expressed by *H. pylori* when the extracellular environment experiences a drop in pH. This Class I nickel–cobalt transporter of the NiCoT family catalyzes the uptake of Ni(II) across the inner membrane from the periplasm. In this study, we characterized NixA using a platform whereby, for the first time on a NiCoT transporter, recombinantly expressed and purified NixA and key mutants in the translocation pathway have been reconstituted in artificial lipid bilayer vesicles (proteoliposomes). Fluorescent sensors responsive to Ni(II) transport (Fluozin-3-Zn(II)), luminal pH changes (pyranine), and membrane potential (oxonol VI) were encapsulated in the proteoliposomes lumen to monitor, in real-time, NixA transport properties and translocation mechanism. Kinetic transport analysis revealed that NixA is highly selective for Ni(II) with no substrate promiscuity towards Co(II), the other putative metal substrate of the NiCoT family, nor Zn(II). NixA-mediated Ni(II) transport exhibited a Michaelis–Menten-type saturable substrate concentration dependence, with an experimental $K_{M,\ Ni(II)} = 31.0 \pm 1.2$ μM. Ni(II) transport by NixA was demonstrated to be electrogenic, and metal translocation did not require a proton motive force, resulting in the generation of a positive-inside transmembrane potential in the proteoliposome lumen. Mutation analysis characterized key transmembrane residues for substrate recognition, binding, and/or transport, suggesting the presence of a three-step transmembrane translocation conduit. Taken together, these investigations reveal that NixA is a Ni(II)-selective Class I NiCoT electrogenic uniporter. The work also provides an *in vitro* approach to characterize the transport properties of metal transporters responsible for Ni(II) acquisition and extrusion in prokaryotes.

Received 28th September 2023
Accepted 29th November 2023

DOI: 10.1039/d3sc05135h

rsc.li/chemical-science

Introduction

Nickel is an essential trace metal present predominantly in prokaryotic (and plant) enzymes.[1–9] Ni(II) participates in the maturation and as catalytic cofactor in metalloenzymes that catalyze challenging chemical reactions, such as in the cases of CODH (carbon monoxide dehydrogenase) and [NiFe] hydrogenase.[1–9] CODH enzymatic activity produces low potential electrons and drive the reversible and selective interconversion of carbon monoxide to carbon dioxide. As a result, CODH activity is central for carbon fixation processes and the survival of organisms possessing CODH.[1–9] [NiFe] hydrogenase catalyzes the reversible conversion of molecular hydrogen to protons and electrons that are needed in critical metabolic pathways.[1–9] To guarantee that the necessary Ni(II) cellular "quotas" are met, bacteria requiring Ni(II) evolved a network of nickel binding proteins that allows selective metal ion uptake, extrusion, delivery, storage, and chaperoning to target metalloenzymes, so that cellular Ni(II) concentrations are tightly controlled to meet the physiological needs without reaching toxic levels.[3–12]

[a]*Department of Chemistry and Biochemistry, The University of Texas at Dallas, Richardson, TX 75080, USA. E-mail: gabriele.meloni@utdallas.edu*

[b]*Laboratory of Bioinorganic Chemistry, Department of Pharmacy and Biotechnology, University of Bologna, Bologna I-40127, Italy*

† Electronic supplementary information (ESI) available. See DOI: https://doi.org/10.1039/d3sc05135h

Helicobacter pylori (*H. pylori*), a Gram-negative bacterium, has been identified as the causative agent of human gastric and duodenal ulcers, both of which can eventually lead to gastric cancer.[4,13] The extremely low pH environment in the stomach, where *H. pylori* replicates, presents a challenge to its survival and replication. *H. pylori* utilizes another key cytosolic nickel-containing metalloenzyme, urease, to cope and persist in this harsh environment. Urease is matured *via* insertion of two Ni(II) ions as cofactors in its catalytic site, to catalyze the hydrolysis of urea to ammonia and carbon dioxide.[14] The produced ammonium and bicarbonate generate a pH-buffered microenvironment that allow *H. pylori* to survive in the acidic milieu of the gastric tissue.[4,11,14] Thus, Ni(II) uptake across its cellular membranes, is crucial for *H. pylori* survival and pathogenicity.[2,4,11,15–17]

In *H. pylori*, ABC (ATP Binding Cassette) transporters and nickel–cobalt permeases (NiCoTs) have been identified to be the prominent transmembrane Ni(II) transporters for nickel acquisition across its inner membrane.[10,17–25] *In vivo* studies on the activity of nickel–cobalt permeases have proven their importance in Ni(II) uptake and urease maturation,[10,11,17–25] but the knowledge regarding their transport properties, such as translocation mechanism, substrate selectivity bias, and transport modality remains to be investigated, as biochemical and biophysical investigations on purified NiCoT transporters are lacking. The Ni(II) uptake pathway to the cytoplasm involves FrpB4, an outer membrane protein supported by the TonB protein, and FecA3, which translocates Ni(II) from the outer membrane to the periplasm.[11,26–28] Subsequently, Ni(II) is transported from the periplasm to the cytoplasm through NixA or the Ni(II) ABC transporter NiuBDE.[17,29,30] Once in the cytoplasm, a complex network of metallochaperones interact with Ni(II) to store this metal ion and mediate nickel-enzymes maturation, as widely investigated for urease and hydrogenase.[3–12]

NixA is known to be a high-affinity nickel transporting protein, facilitating the import of Ni(II) across the inner membrane in *H. pylori*.[17,29,30] NixA is a member of the NiCoT importer family.[10,17–25,29,30] These permeases feature several subclasses based on their substrate preference towards the metal substrates Ni(II) and Co(II). The family is postulated to consist of at least three transporter groups, where Class I appear to be exclusively selective for Ni(II). Classes II and III appear to be instead promiscuous, and catalyze the translocation of both Ni(II) and Co(II), but with a preferential selectivity bias for Co(II) or Ni(II), respectively.[21,31] NixA is classified as a Class I NiCoT, and expected to exclusively transport Ni(II) based on *in vivo* evidence.[20,31]

Existing studies have determined NixA activity through indirect *in vivo* methods such as metal accumulation analysis (liquid scintillation) and urease activation assays upon cellular exposure to different metals.[30,32] NixA has been observed to selectively transport Ni(II) while discriminating against other divalent cations such as Zn(II), Co(II), and Cu(II).[6] Eight putative transmembrane helices (TM) are conserved across all proteins in the NiCoT family and it has been proposed that TMs II and III are responsible for the transport activity of NixA. Mutation of amino acids located in TMs II (H44, D47, D49, D50, D55) and III (H79), believed to be critical for NixA activity, to isoleucine, reduce Ni(II) uptake and urease activity *in vivo*.[29,30,32] Despite the crucial role of NixA in the survival of *H. pylori*, the molecular mechanism by which the protein facilitates Ni(II) transport remain to be fully elucidated.

Biochemical and biophysical characterization of the transport properties on purified NiCoT systems, including NixA, are currently lacking due to the limitations of methodologies to express and purify NiCoTs in active forms, and shortage of molecular tools that allow direct measurement of substrate translocation, co-/counter-ion transport, and electrogenicity with transporter reconstituted in native-like membranes.

This work describes an effort to fill this gap, through the development of a platform to recombinantly express and purify NixA for reconstitution in artificial lipid bilayers (small unilamellar vesicles (SUVs), also called proteoliposomes). Through this platform, which mimics the biophysical properties of cellular membranes, we determined key NixA transport properties. Three liposome-compatible and impermeable fluorescent probes were encapsulated in the proteoliposomes' lumen to characterize NixA metal translocation mechanism and kinetics: (1) a Ni(II)-sensitive fluorescent probe, Fluozin-3-Zn(II) (FZ-3-Zn),[33–36] (2) the pH sensitive probe pyranine,[37] (3) and the membrane potential sensor oxonol VI.[38] Based on transport assays, we determine that NixA is a highly-selective, high-affinity Ni(II) uniporter, and that metal transport is electrogenic. By mutational analysis, coupled to metal binding determinations and transport assays, we also identified and dissected key residues in the putative NixA transmembrane translocation pathway that control Ni(II) recognition, selection and transport across the lipid bilayer, thus providing novel molecular insight in the transport properties of NixA. While the use of proteoliposomes with encapsulated fluorescent probes responsive to diverse stimuli in the lumen has been utilized to the study of other metal transporters, in this work we developed a novel methodology that allows these investigations to study Ni(II) transmembrane transporters, opening the venue for the characterization of the translocation properties in real-time of other Ni(II)/Co(II) transporter families upon their reconstitution in native-like artificial lipid bilayers.

Materials and methods

Expression and purification of wild-type NixA and inactive mutants

Synthetic DNA encoding codon-optimized wild-type NixA (wtNixA Uniprot: Q48262) from *H. pylori* was synthetized and cloned in a pET-52b(+) vector between the SmaI and SacI restriction sites (Genscript Inc.), generating a construct encoding a thrombin cleavage site followed by a His-10-tag at the protein C-terminus. Single-point and combination mutants were commercially generated by Genscript Inc. following a proprietary mutagenesis strategy. Mutant's constructs were verified by sequencing using primers listed in ESI Table S1.† Plasmids were transformed in *E. coli* BL21 (DE3) GOLD (Agilent Technologies) and clones selected on Luria Broth agar (LB-agar)

plates after O/N growth at 37 °C. Precultures were prepared in Terrific Broth (TB) media by O/N growth at 37 °C. The main cultures, in TB-media supplemented with 1% glycerol, were inoculated with precultures at 1% (v/v). Cells were grown in the presence of 50 μg mL^{-1} ampicillin, under constant shaking (140 rpm), at 37 °C. The OD_{600} was recorded regularly, and the temperature was decreased to 23 °C when OD_{600} reached a value of 2, both for the expression of both wild-type NixA (wtNixA) and related mutants. After 1 h, 0.1 mM isopropyl thiogalactopyranoside (IPTG) was added to the cultures and the target proteins were expressed at 23 °C for 16 h, at 140 rpm.

Cells were harvested by centrifugation, at 4000×*g* for 25 min at 4 °C (Thermo Scientific Sorvall LYNX 6000 centrifuge). The cells were resuspended in lysis buffer (20 mM Tris/HCl, pH 8, 100 mM NaCl, 5 mM $MgCl_2$, 30 μg mL^{-1} deoxyribonuclease I from bovine pancreas (Sigma-Aldrich) and 2× EDTA-free protease inhibitor cocktail tablets (Thermo Scientific)). The cells were lysed at a low temperature (~4 °C) using a microfluidizer (Microfluidics M-110P) at 20 000 psi by three passages through a Z-shaped diamond chamber cooled on ice. The lysate was centrifuged at 17 000×*g* for 25 min at 4 °C (Thermo Scientific Sorvall LYNX 6000 centrifuge) to remove cell debris. The supernatant was collected and subjected to ultracentrifugation (37 000 rpm, 1 h, 4 °C) to isolate the cell membrane fraction that contained wtNixA or its mutants. The membrane pellet was resuspended in storing buffer (20 mM Tris/HCl, pH 8, 500 mM NaCl, 1% glycerol (w/v), 1× EDTA-free protease inhibitor cocktail tablets (Thermo Scientific)) to a final membrane concentration of 1.0 g of cells per 1.0 mL of buffer. The membrane suspension was subsequently frozen in liquid N_2 and stored at −80 °C until protein purification.

For purification, 10 mL of the membrane suspensions were mixed with 40 mL of membrane resuspension buffer (20 mM Tris/HCl pH 8.0, 500 mM NaCl, 1× EDTA-free protease inhibitor cocktail tablets (Thermo Scientific), 25 mM imidazole, 5 mM β-mercaptoethanol). To solubilize the membrane proteins, *n*-tetradecylphosphocholine (Fos-choline-14) was added to the membrane suspension to a final concentration of 1% (w/v), and the mixture stirred for 1 h, at 4 °C, to guarantee wtNixA/mutants extraction. The suspension was subsequently subjected to ultracentrifugation (37 000 rpm, 1 h, 4 °C; Beckman Optima XPN80) to separate the solubilized membrane protein fraction from the residual membrane debris. Afterwards, the supernatant was loaded to a Ni-NTA HisTrap FF column pre-equilibrated with binding buffer (20 mM Tris/HCl pH 8.0, 500 mM NaCl, 25 mM imidazole, 1 mM tris(2-carboxyethyl) phosphine (TCEP), 0.05% (w/v) Fos-choline-14), using an AKTA Pure FPLC system (Cytiva). The column was washed with 30 column volumes (CV) of wash buffer (20 mM Tris/HCl pH 8.0, 500 mM NaCl, 25 mM imidazole, 1 mM TCEP, 0.05% (w/v) Fos-choline-14), to remove unbound proteins and impurities. The bound proteins were eluted with a 5 CV linear imidazole gradient (0–100%) generated by mixing wash buffer and elution buffer (20 mM Tris/HCl pH 8.0, 500 mM NaCl, 500 mM imidazole, 1 mM tris(2-carboxyethyl) phosphine (TCEP), 0.05% (w/v) 7-cyclohexyl-1-heptyl-β-D-maltoside (CYMAL-7)). The fractions containing NixA were collected and concentrated to ~5–10 mg mL^{-1} using 30 000 Da MWCO cutoff filter (Sartorius VIVASPIN 20) *via* centrifugation (4000×*g*, 4 °C). The protein was further purified through a size exclusion chromatographic (SEC) step, by loading the protein solution onto a Superdex 200 Increase 10/300 column equilibrated with 20 mM MOPS/NaOH buffer, pH 7.0, 500 mM NaCl, 1 mM TCEP and 0.05% (w/v) CYMAL-7. The SEC fractions containing wtNixA/mutants were eluted using the same buffer, collected and concentrated to ~1–5 mg mL^{-1}.

The purity of the obtained protein was verified by SDS-PAGE (4–15% Tris-Glycine Mini-PROTEAN gels, BioRad) and western blot analysis utilizing an antibody recognizing the His_{10}-tag present at the C-terminus (6x-His Tag Monoclonal Antibody, HIS.H8, Invitrogen). The protein concentration was determined from the absorbance at 280 nm measured with a Nanodrop spectrophotometer (Thermo Scientific Nanodrop One), given the extinction coefficient of $\varepsilon_{280} = 43\,890\ M^{-1}\ cm^{-1}$ for wild-type NixA. The protein was frozen in liquid N_2 and stored at −80 °C until further use. All mutants were expressed and purified following the same protocol of wtNixA.

Small-scale detergent screening

A small-scale detergent optimization was performed to identify the optimal detergent to be used for membrane protein extraction. 200 μL of isolated membranes were mixed with 800 μL of membrane resuspension buffer (20 mM Tris/HCl pH 8.0, 500 mM NaCl, 1× EDTA-free protease inhibitor cocktail tablets (Thermo Scientific), 25 mM imidazole, 5 mM β-mercaptoethanol). Detergent stock solutions (DMNG: decyl maltose neopentyl glycol; FC-14: Fos-choline-14; CYMAL-7: 7-cyclohexyl-1-heptyl-β-D-maltoside; LDAO: lauryldimethylamine-*N*-oxide; OG: *n*-octyl-β-D-glucopyranoside; DDM: *n*-dodecyl-β-D-maltopyranoside) were added to individual membrane mixtures at a final 1% (w/v). The mixtures were homogenized using a Benchmark D1000 homogenizer. The suspension was incubated for 1 h, at 4 °C, while tilting. The membrane solutions were then subjected to ultracentrifugation at 150 000×*g* for 30 min at 4 °C (Sorvall mX120+ Micro-Ultracentrifuge) to separate the solubilized supernatant and the insoluble membrane pellet. The supernatant and pellet were then analyzed *via* western blot and SDS-PAGE.

His_{10}-tag removal for Ni^{2+}-binding stoichiometry determination

The histidine-tag was removed from the purified wtNixA by addition of bovine Thrombin (20 units per mg NixA; EMD Millipore Crop) to a final 1 : 5 protein : thrombin (v/v) ratio. The cleavage was carried out at 21 °C for 10 h, under constant shaking. Thrombin and other impurities were removed by SEC, using a pre-equilibrated Superdex 200 Increase 10/300 column, and eluted with 20 mM MOPS/NaOH buffer, pH 7.0, 500 mM NaCl, 1 mM TCEP, 0.05% (w/v) CYMAL-7.

NixA and mutants reconstitution in liposomes

Liposomes were prepared by mixing L-α-phosphatidylcholine from chicken egg (Avanti Polar Lipids) and *E. coli* polar lipids extract (Avanti Polar Lipids) at a 1 : 3 ratio (w/w). The lipid mixture, dissolved in chloroform, was dried using a stream of

nitrogen gas under rotation and residual solvent was removed overnight in a vacuum desiccator.

The dried lipid cake was hydrated and resuspended using a Chelex®-treated (BioRad) solution of 1 mM TCEP in MilliQ H_2O. The lipid suspension was buffered to final 20 mM MOPS/NaOH, pH 7, 100 mM NaCl, 1 mM TCEP, using a Chelex®-treated 10× buffer stock (200 mM MOPS/NaOH, pH 7, 1 M NaCl, 1 mM TCEP). The lipids suspensions were prepared to a final total lipid concentration of 25 mg mL^{-1}.

Liposomes were prepared by subjecting the lipid suspension to three freeze–thaw cycles in liquid nitrogen, followed by sequential 11 extrusions through polycarbonate (PC) membranes of decreasing pore sizes (1 μm, 0.4 μm then 0.2 μm filters), using a 1 mL airtight syringe system (Avanti, Polar Lipids, Inc.) to produce unilamellar vesicles. The liposomes suspensions were collected and subsequently destabilized by addition of CYMAL-7 detergent at a final concentration of 0.02% (w/v) and incubation for 1 h, at room temperature, under tilting, prior to protein incorporation. Purified wtNixA and mutants (~1–5 mg mL^{-1}) were reconstituted into the liposomes by adding purified proteins stocks to a final 1 : 25 (w/w) protein : lipid ratio. Similarly, control liposomes were prepared by buffer addition to the detergent destabilized liposomes.

The liposome and protein mixtures, as well as the control liposomes, were tilted for 1 h at 4 °C. The CYMAL-7 detergent was removed using Bio-Beads (SM-2; BioRad). The Bio-Beads were activated *via* consecutive washings with methanol, ethanol, and water, followed by drying through vacuum filtration. The activated Bio-Beads were added to the proteoliposomes and the control liposome to a final concentration of 60 mg mL; then, the mixtures were tilted for 1 h at 4 °C for the first Bio-Bead exchange prior to subsequent BioBead resin exchanges carried out for 12, 14, and 16 h.

The prepared liposomes were collected by ultracentrifugation at 180 000×*g* for 30 min at 4 °C (Sorvall mX120+ Micro-Ultracentrifuge). The pellets were collected and resuspended in 20 mM MOPS/NaOH, pH 7, 100 mM NaCl, 1 mM TCEP (Chelex®-treated), to a final total lipid concentration of 25 mg mL^{-1} (wtNixA/mutants = 1 mg mL^{-1}). In order to assess the level of protein incorporation in the proteoliposomes, SDS-PAGE (4–15% Tris-Glycine Mini-PROTEAN gels, BioRad) densitometric analysis was performed on the supernatant and the resuspended proteoliposomes.

The proteoliposomes and the control liposomes were frozen in liquid N_2 and stored at −80 °C.

The number of NixA molecules incorporated in each proteoliposome particle was estimated by determining the SUV diameter by dynamic light scattering and knowing the lipid concentration, under the assumption that the SUVs are spherical particles.[35] The total lipid head group area (S_{TOT}) can be calculated as the sum of the proteoliposome outer layer surface area (S_{out}) and the inner layer surface area (S_{in}). The bilayer thickness is approximately 3 nm (h = 3 nm), and S_{TOT} can be calculated as:

$$S_{TOT} = S_{out} + S_{in} = 4\pi r^2 + 4\pi(r - h)^2$$

The total number of lipid molecules per proteoliposome (N_{TOT}) can be estimated from S_{TOT} and the average polar head surface (S_L 0.7 nm^2 per phospholipid):

$$N_{TOT} = S_{TOT}/S_L$$

Assuming that the average molecular weight of phospholipids is 750 g mol^{-1}, the approximate molecular weight of single proteoliposome was obtained. The number of NixA molecules per SUV was subsequently calculated knowing the concentrations of lipids and protein in the proteoliposome preparations.

Determination of SUV's size distribution by dynamic light scattering (DLS)

The size distribution of the NixA proteoliposomes and control liposomes were obtained by UV-Vis Dynamic Light Scattering (DLS) with a Zeta Sizer Nano ZS DLS instrument (Malvern Panalytical). The samples were placed in a polystyrene cuvette and the measurements conducted at 25 °C, at a scattering angle of 175°, with a laser wavelength of 633 nm (refractive index of sample medium = 1.33 and refractive index of material = 1.45).[35] The polydispersity index (PDI) for control liposome and NixA proteoliposomes were 0.066 and 0.153 respectively.

Fluozin-3-Zn(II) probe encapsulation in SUVs and *in vitro* Ni(II) transport assays

Control liposomes and proteoliposomes carrying wtNixA and its mutants were diluted to a final concentration of 12.5 mg mL^{-1} in the transport buffer (20 mM MOPS/NaOH, pH 7, 100 mM NaCl, 1 mM TCEP). Equimolar amounts of Fluozin-3 (final concentration = 10 μM) and Zn(II) (10 μM) were added to the suspensions, and the Fluozin-3-Zn(II) complex was encapsulated in the lumen by membrane freeze-fracture upon three freeze–thaw cycles in liquid nitrogen. Liposomes were subsequently sequentially extruded through 1 μm and 0.2 μm PC membrane filters using an airtight syringe system. The unencapsulated Fluozin-3-Zn(II) complex was removed by ultracentrifugation at 160 000×*g* for 45 min at 4 °C in a Sorvall mX120+ Micro-Ultracentrifuge. The pellets were collected and washed with the transport buffer (1 mL), collected *via* a subsequent ultracentrifugation step, and subsequently recollected and resuspended in the transport assay buffer (20 mM MOPS/NaOH, pH 7, 100 mM NaCl, 1 mM TCEP). The control liposomes were subjected to the same protocol.

Buffer solutions (20 mM MOPS/NaOH, pH 7, 100 mM NaCl, 1 mM TCEP) and Chelex®-treated MilliQ water were made oxygen-free on a Schlenk-line by at least four vacuum/nitrogen gas cycles. Stock solutions of Ni(II) were freshly prepared in an aerobic glove box with constant nitrogen gas flow. The Ni(II) stock solutions were prepared from a 0.1 M $NiCl_2$ stock solution. 100× Ni(II) stocks (100 μM–10 mM) for transport assay were prepared *via* dilution in oxygen-free transport buffer. The stock solutions were stored in a sealed tube prior to use.

The Ni(II) transport assays were conducted at 25 °C using a spectrofluorometer (Horiba Scientific Fluoromax-4) at excitation (λ_{exc}) and emission (λ_{exc}) wavelengths of 480 nm (slit widths: 2.5 nm) and 515 nm (slit widths: 2.5 nm), respectively. NixA proteoliposomes (120 μL), with the encapsulated Fluozin-3-Zn(II) probe complex, were placed in a sub-micro quartz cuvette and the baseline fluorescence was collected for 50 s prior to the addition of Ni^{2+}.

Ni(II) transport was triggered by the addition of 1.2 μL Ni(II) stock solutions and the fluorescence signal change monitored for 500 s at 0.1 s intervals. Ni(II) transport was determined by plotting the $\Delta F/F_0$ *versus* time, where ΔF is the difference between the fluorescence measured at time t (F_t) and the fluorescence immediately before Ni(II) addition (F_0). The same protocol was utilized for the characterization of control liposomes and NixA mutants.

Ni(II)/H^+ co-/counter-ion transport monitored by pH sensitive probe pyranine

Control liposomes and proteoliposomes carrying wtNixA and its mutants were diluted (1 : 2 (v/v)) in the transport buffer (4 mM MOPS/NaOH, pH 7, 100 mM NaCl, 1 mM TCEP). Subsequently, a 20 mM pyranine stock solution in H_2O (Alfa Aesar) was added to a final concentration of 1 mM. The pH sensitive probe was encapsulated through three freeze–thaw cycles, followed by consecutive extrusion through 1 μm, 0.4 μm, and 0.2 μm PC membrane filters using gas-tight syringes. The proteoliposome and control liposome pellets were collected by ultracentrifugation (160 000×*g*, 45 min, 4 °C, Sorvall mX120+ Micro-Ultracentrifuge), and the supernatant containing excess pyranine removed. The proteoliposome pellets and control liposomes were washed using the transport buffer (1 mL) to further remove any unencapsulated pyranine excess. Pellets were collected by ultracentrifugation (180 000×*g*, 30 min, 4 °C; Sorvall mX120+ Micro-Ultracentrifuge) and resuspended in the same transport buffer for H^+ counter-ion transport assays.

The H^+ co-/counter-ion transport assays were conducted as described for the Ni(II) transport assays. The reaction was triggered by addition of 1.2 μL of Ni(II) stocks (100×; 2.5 mM) to NixA proteoliposomes and control liposomes. The fluorescence signal change was monitored for 500 s at 0.1 s intervals (λ_{exc}: 480 nm, slit width: 1 nm; λ_{em}: 515 nm, slit width: 1 nm). Kinetics were reported by plotting $\Delta F/F_0$ as a function of time.

Ni(II) transport electrogenicity monitored with the membrane potential probe oxonol VI

Control liposomes and proteoliposomes carrying wtNixA and its mutants were diluted to a final lipid concentration of 12 mg mL^{-1} in the transport buffer (20 mM MOPS/NaOH pH 7, 100 mM NaCl, 1 mM TCEP). The membrane potential fluorescent probe oxonol VI, which can detect transmembrane potential changes, was added to the suspension to a final concentration of 5 μM. Oxonol VI was encapsulated into the proteoliposomes and control liposomes by three freeze–thaw cycles in liquid N_2, followed by sequential extrusion through 1 μm, 0.4 μm, and 0.2 μm PC membrane filters using gas-tight syringes. The suspension was centrifuged (160 000×*g*, 45 min, 4 °C, Sorvall mX120+ Micro-Ultracentrifuge) to collect proteoliposome/liposome pellets and remove the unencapsulated oxonol VI in the supernatant. The pellets were further washed with the transport buffer (1 mL) to remove the excess probe. The pellets were collected by ultracentrifugation (160 000×*g*, 45 min, 4 °C, Sorvall mX120+ Micro-Ultracentrifuge)) and subsequently resuspended in the same buffer.

The membrane potential transport assays were conducted as described for the Ni(II) transport assays. Proteoliposomes or control liposomes (120 μL) were placed in a sub-micro quartz cuvette and equilibrated at 25 °C. Subsequently, 1.2 μL Ni(II) stock solutions (100×; 2.5 mM) were added to trigger substrate transport. The fluorescence signal was monitored for 500 s at 0.1 s intervals (λ_{exc}: 580 nm, slit width: 4 nm; λ_{Em}: 660 nm; slit width: 5 nm). Kinetics of transmembrane potential changes were reported by plotting $\Delta F/F_0$ as a function of time.

wtNixA and mutants Ni(II)-binding stoichiometry determination

Prior to the binding experiments, purified wtNixA and its mutants were incubated with EDTA to a final concentration of 1 mM. Subsequently, EDTA was removed by injecting the protein samples on a SEC column (Superdex 200 10/300 Increase) and eluted using a Chelex®-treated SEC buffer (20 mM MOPS/NaOH, pH 7.0, 500 mM NaCl, 1 mM TCEP, 0.05% (w/v) CYMAL-7). Subsequently, wtNixA and its mutants were concentrated to at least 10 μM by centrifugation using 30 000 Da MWCO cutoff filter concentrators (Sartorius VIVASPIN 20; 4000×*g*, 4 °C). The concentration of the protein was determined by absorbance at 280 nm on a Nanodrop spectrometer (Thermo Scientific Nanodrop One). Three Ni(II) equivalents ($NiCl_2$) dissolved in Chelex®-treated SEC buffer (20 mM MOPS/NaOH, pH 7.0, 500 mM NaCl, 1 mM tris(2-carboxyethyl) phosphine (TCEP), 0.05% (w/v) 7-cyclohexyl-1-heptyl-β-D-maltoside (CYMAL-7)), were added to the metal-free protein sample (500 μL; 10–20 μM). The mixture was incubated for 10 min at room temperature under shaking. Protein samples were injected in a SEC column (Superdex 200 10/300 Increase) to remove the unbound Ni(II). The protein eluate (1.4 mL) was collected and analyzed by SDS-PAGE (4–15% Tris-Glycine Mini-PROTEAN gels, BioRad) to confirm the presence of protein. To determine the binding stoichiometry (metal : protein ratio), the metal concentration was determined by Inductively Coupled Plasma Mass Spectrometry (ICP-MS) and the protein concentration by a Bradford assay.

The protein eluate aliquots (100 μL) were digested in concentrated HNO_3 overnight. The mixture was diluted to 2 mL using Chelex®-treated water. The Ni(II) concentration was determined using ICP-MS on a 7800 Inductively Coupled Plasma Mass Spectrometer (Agilent), equipped with an autosampler. Prior to the Ni(II) analysis, Ni(II) standards (Nickel Standard for ICP-MS by Sigma Aldrich) were prepared in 2% HNO_3 to generate a calibration curve.

To determine the protein concentration, protein samples (4 μL) were mixed with of 1.0 M NaOH (4 μL) and Bradford reagent

(192 μL). The absorbance at 595 nm was determined using a plate reader (TECAN Spark Multimode Microplate Reader), and protein concentrations calculated using a standard calibration curve generated using a purified NixA stock with a known concentration.

Isothermal titration calorimetry

The thermodynamics of Ni(II) binding to wtNixA was investigated using isothermal titration calorimetry (ITC). Titrations were performed using a high-sensitivity VP-ITC microcalorimeter (MicroCal LLC, MA, USA.), at 25 °C. The reference cell of the microcalorimeter was filled with MilliQ water. A 20 μM wtNixA solution in Chelex®-treated buffer containing 20 mM MOPS buffer, 500 mM NaCl, 1 mM TCEP, 0.05% CYMAL-7, at pH 7.0, loaded into the sample cell (1.4093 mL), was titrated by performing forty 5 μL injections of a 0.4 mM $NiCl_2$ solution, dissolved in the same buffer, using a computer-controlled microsyringe. A control experiment was carried out, under identical conditions, by titrating the $NiCl_2$ solution into buffer alone, to exclude any significant heat of dilution. The integrated heat data obtained for the titration were fitted using the AFFINImeter software,[39] carrying out a nonlinear least-squares minimization of two alternative models, namely (i) a stoichiometric equilibria (SE) model, or (ii) an independent sites (IS) model. The SE model is based on stoichiometric (or macroscopic) equilibrium constants and is typically applied when the different binding sites are coupled to each other; the IS model is based on site-specific (or microscopic) equilibrium constants relative to different binding sites that do not influence each other.[39] The molar enthalpy change (ΔH, cal mol^{-1}) and binding constant (K_a, M^{-1}) were the floating thermodynamic parameters in the fit.[39] The parameters r_M (scaling parameter for the protein concentration) and Q_{dil} (heat of dilution, cal mol^{-1}) were also adjusted as fitting parameters. The molar entropy change was calculated using the relationships $\Delta G = -RT \ln K_a$ ($R = 1.9872$ cal mol^{-1} K^{-1}, $T = 298$ K) and $\Delta G = \Delta H - T\Delta S$. The statistical goodness of fit (GoF) parameter was used to assess the best fit.

Results and discussion

Recombinant NixA expression in *E. coli*, purification, and reconstitution in SUVs

We developed a methodology to express NixA in *E. coli* recombinant cells using a codon-optimized construct encoding for the amino acid sequence from *H. pylori* (Uniprot: Q48262). Protein expression was maximized in BL21(DE3)-Gold *E. coli* cells. The membranes from the lysed cells expressing NixA were isolated by ultracentrifugation, followed by solubilization of membrane proteins using a biocompatible detergent. Prior to develop a purification strategy, a small-scale detergent screen, utilizing six detergents classes with different polar head and/or hydrophobic tails, was conducted to identify an ideal molecule to guarantee the highest NixA membrane extraction efficiency (ESI Fig. S1†). The zwitterionic Fos-choline-14 was selected as the most efficient detergent for extraction, as demonstrated by SDS-PAGE analysis of the solubilized fraction *vs.* the insolubilized NixA in the membrane pellet isolated by ultracentrifugation. The NixA construct was designed to encode a C-terminal poly-histidine tag, and the first purification step was performed by Immobilized Metal Affinity Chromatography (IMAC). IMAC purification yielded 5–10 mg NixA per liter of culture, with >90% purity as determined by SDS-PAGE analysis (ESI Fig. S2†). The protein eluate was subsequently further purified by Size Exclusion Chromatography (SEC), allowing to switch the detergent to cyclohexyl-1-heptyl-β-D-maltoside (CYMAL-7), a milder polar non-charged maltoside detergent. This exchange proved to be critical in minimizing protein aggregation. SEC analysis revealed monodispersed NixA-CYMAL-7 micelle complexes with no significant aggregation (Fig. 1A). This protocol allowed micellar NixA purification in monomeric form to >95% purity, as demonstrated by SDS-PAGE and western blot analysis (Fig. 1B).

To generate NixA proteoliposomes and control liposomes, artificial lipid bilayer SUV vesicles were generated by extrusion, and the obtained liposomes destabilized by CYMAL-7 addition, followed by the incorporation of NixA at a 1 : 25 protein/lipid (mg mL^{-1}) ratio. Leakage-free proteoliposomes were obtained upon detergent removal with BioBeads SM2 resin. Characterization of control liposomes and NixA proteoliposomes by Dynamic Light Scattering (DLS) revealed monodisperse size distributions, with average diameters of 163 ± 53 nm and 156 ± 65 nm, respectively (Fig. 1C). The amount of reconstituted NixA in the proteoliposomes was determined by SDS-PAGE densitometric analysis, upon ultracentrifugation to remove non-reconstituted proteins. NixA quantification in both the soluble and proteoliposome pellet fractions (Fig. 1D) revealed successful reconstitution, with >95% NixA incorporation in the lipid bilayer. Further, based on the average size of the NixA proteoliposomes and the ratio of protein-to-lipid reconstitution, the number of NixA molecules incorporated in each SUV was estimated as approximately 150 molecule per vesicle.

Ni(II) transport monitored by FZ-3-Zn(II) probe complex

The biochemical and biophysical transport properties of NixA, such as its translocation mechanism, substrate selectivity, and kinetics, have not yet been fully established due to the absence of an appropriate platform to study substrate translocation events in purified Ni(II)-transporters. Previous studies attempting to address its transport mechanism were based on *in vivo* studies of membrane extracts with radiolabeled metals, and *in vivo* urease assays to indirectly quantify the NixA activity.[29,30,32] Analysis on crude membrane extracts and indirect urease activity assays remain of challenging interpretation as a result of the activity of other promiscuous metal protein transporters for the same metal substrate, resulting in possible interferences. Moreover, real-time kinetics determinations of Ni(II) transport are lacking in literature due to the scarcity of highly-sensitive, lipid-compatible, and impermeant fluorescent probes that can be encapsulated in small unilamellar vesicles to detect Ni(II) translocation.

We thus established a fluorescent-probe screening procedure to identify a suitable fluorescent probe that could detect the desired metal substrate when encapsulated inside the

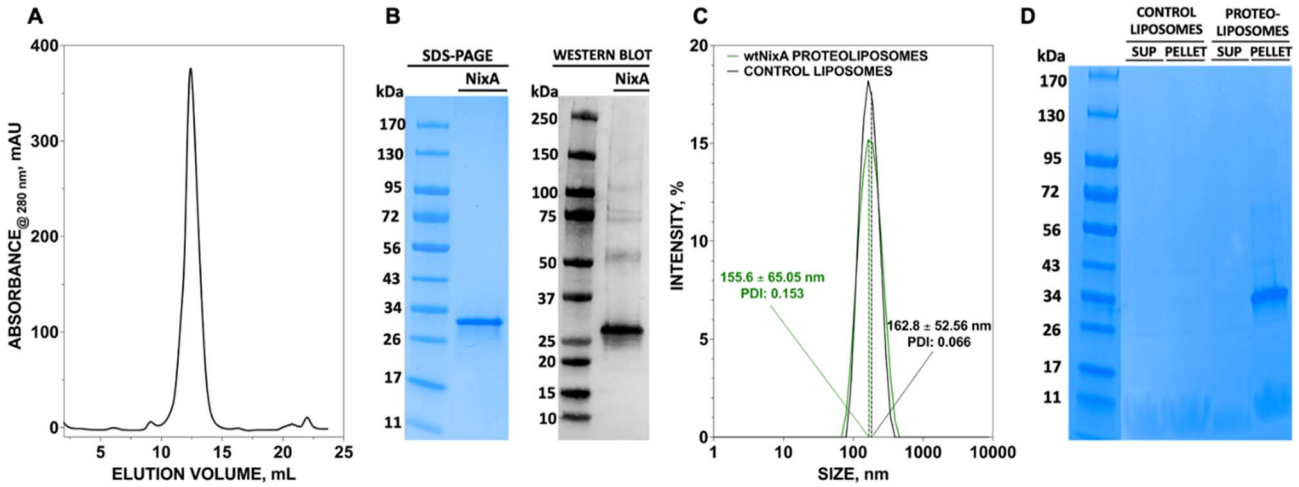

Fig. 1 Purification of NixA and reconstitution in proteoliposomes. (A) Size exclusion chromatogram profile of NixA purified in CYMAL-7 micelles, and (B) SDS-PAGE of purified NixA after SEC, and corresponding and western blot analysis utilizing an Anti-His_6 tag monoclonal antibody. (C) Dynamic light scattering (DLS) analysis of control liposomes and NixA proteoliposomes showing the monodisperse size of SUVs and corresponding polydispersity index (PDI). (D) SDS-PAGE analysis of NixA reconstitution in the proteoliposome fraction isolated by ultracentrifugation (pellet) compared to non-incorporated soluble NixA (supernatant, SUP), and corresponding control liposomes.

liposomal lumen. The turn-on fluorescent probe Fluozin-3 was initially developed to detect Zn(II) in cellular systems.[33] Application of FZ-3 in monitoring other transition metals revealed a turn-on fluorescent response with other substrates such as Fe(II), Co(II), Ni(II) and Cd(II) in the presence and absence of lipids.[35,36] However, in the putative application of FZ-3 to detect Ni(II) transport activity by NixA in proteoliposomes potential problems were encountered related to: (i) residual Zn(II) contamination in lipids isolated from native sources, and (ii) the FZ-3 significantly higher sensitivity for Zn(II) compared to Ni(II), which would affect batch-to-batch reproducibility. To circumvent these potential problems, we decided to exploit the comparable affinities of FZ-3 for Zn(II) and Ni(II) (or Co(II)), and the significantly lower fluorescent turn-on response (fluorescence yield) for FZ-3-Ni(II)/Co(II) complexes (compared to FZ-3-Zn(II)).[34] We thus mixed Zn(II) with FZ-3 (1 : 1 stoichiometric ratio) to generate FZ-3-Zn(II), and encapsulated it in the proteoliposome lumen. We hypothesized that encapsulation of FZ-3-Zn(II) would result in a significant fluorescence quenching response in case of Ni(II) translocation, resulting from the metal-swapping of Zn(II) with Ni(II) in the FZ-3-metal complex, together with potential collisional quenching contributions. Control experiments conducted by titrating FZ-3-Zn(II) with Ni(II) and Co(II) in lipid environments confirmed a concentration-dependent significant fluorescence quenching upon exposure of FZ-3-Zn(II) to Ni(II) and Co(II) (ESI Fig. S3†). These data substantiate the use of FZ3-Zn(II) as a probe to detect Ni(II) or Co(II) translocation events by NixA, when encapsulated in proteoliposomes (Fig. 2A).

The Ni(II) translocation in NixA proteoliposomes was monitored by recording the fluorescence immediately after the addition of the metal substrate to the proteoliposome solutions at the emission maximum of the FZ-3-Ni(II) complex (λ_{exc} = 480 nm; λ_{em} = 515 nm). The kinetic traces obtained from NixA proteoliposomes revealed a time-dependent development of the fluorescence quenching signal, with a signal equilibration reached approximately after 5–8 min (Fig. 2B). The quenching fluorescence signals were also corrected by subtracting the almost negligible background signals of the corresponding control liposomes. These kinetic traces are indicative of a real-time detection of NixA-mediated Ni(II) transport events across the proteoliposome lipid bilayer. The $\Delta F/F_0$ traces as a function of time showed increasing and faster quenching response upon exposure of the proteoliposomes to increasing extravesicular Ni(II) concentrations, ranging from 1 to 100 μM (Fig. 2B). Exponential fitting of the Ni(II) transport traces was applied to establish apparent initial transport rates ($\delta F/\delta t$) (Fig. 2C inset). The apparent initial velocities obtained revealed a saturable hyperbolic dependency resulting from NixA-dependent Ni(II) transport. The slopes from the kinetic traces at different Ni(II) concentrations were fitted with a Michaelis–Menten-like equation, resulting in a $K_{M,\ Ni(II)} = 31.0 \pm 1.2$ μM and a $(\delta F/\delta t)_{MAX} = -0.0089 \pm -0.0004\ s^{-1}$ (Fig. 2C). The equilibrium fluorescence quenching response values ($\Delta F/F_0$) were also analyzed and fitted with a Michaelis–Menten-like equation, which revealed a similar $K_{M,\ Ni(II)} = 26.6 \pm 1.5$ μM and a $(\Delta F/F_0)_{MAX} = -0.52 \pm -0.01\ s^{-1}$ (Fig. 2C).

Based on previous *in vivo* metal accumulation assays, NixA was tentatively classified as a Class I NiCoT protein, suggesting that NixA might selectively transport only Ni(II) but not Co(II), despite belonging to the NiCoT family.[20,21,31] We thus investigated the metal selectivity of NixA in our proteoliposome system by monitoring the transport of Ni(II) and Co(II) in control liposomes and NixA proteoliposomes. In parallel, we also investigated the transport properties of NixA towards Zn(II), a more abundant non-substrate essential transition metal ion, *via* encapsulation of metal-free FZ-3, which possesses high zinc affinity (K_d ~15 nM) and dramatic turn-on fluorescent response (>50-fold). Transport assays were conducted by supplementing the metal substrates, and by recording the proteoliposome

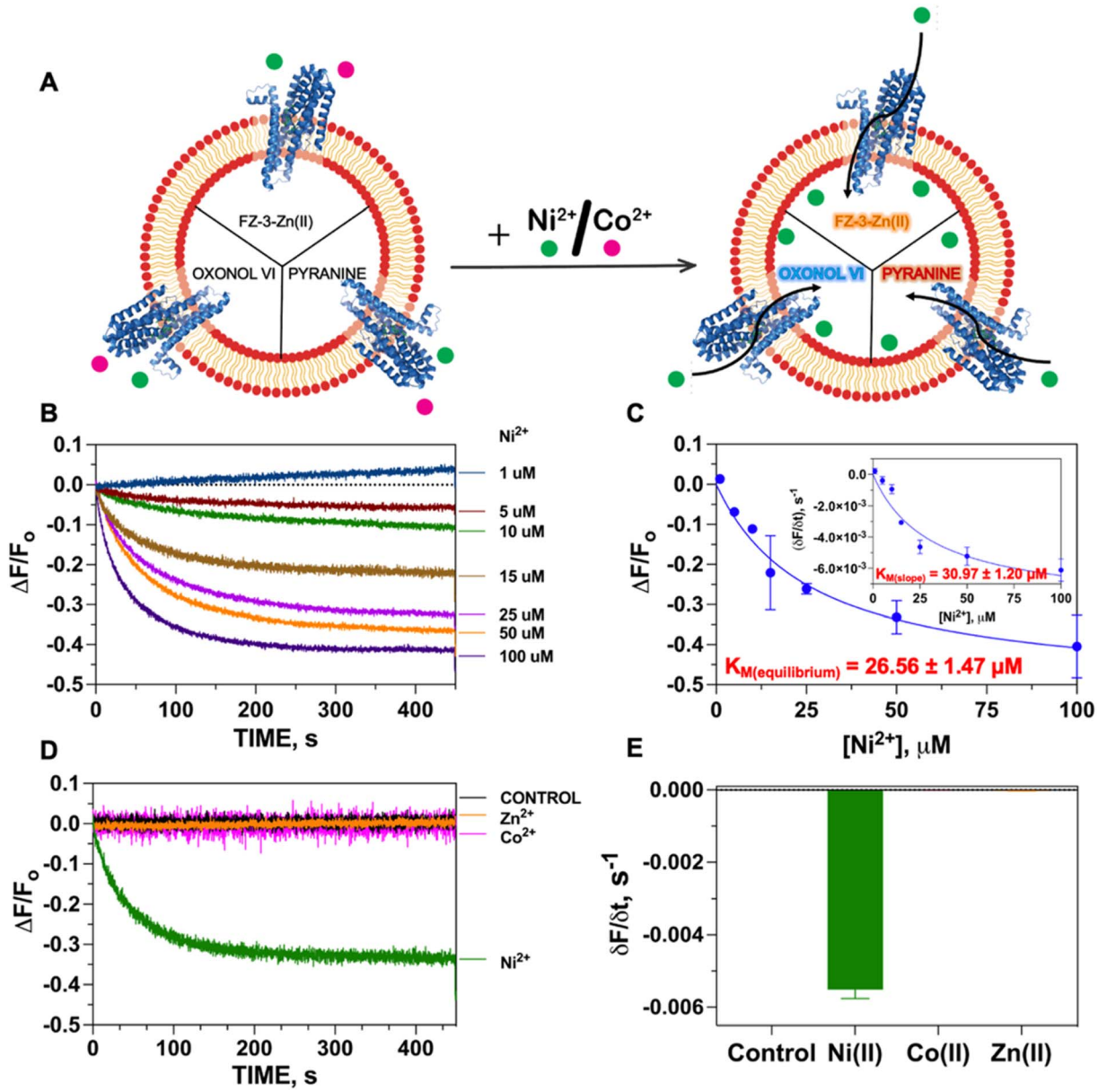

Fig. 2 Transport activity of NixA monitored by FZ-3-Zn(II) complex. (A) Overall scheme for the characterization of NixA transport properties utilizing fluorescent probes responsive to diverse stimuli. (B) Fluorescence quenching transport traces indicative of Ni(II) transport by NixA in proteoliposomes, as monitored by FZ-3-Zn(II) encapsulated in the SUV lumen, as a function of increasing Ni(II) concentrations (1–100 μM; λ_{exc} = 480 nm; λ_{em} = 515 nm) (n = 3). Traces are plotted as differential fluorescence at time t ($F_t - F_0$; ΔF) normalized to the fluorescence prior to the addition of Ni(II) (F_0), with traces corrected by subtracting the signals obtained with control liposomes. (C) Michaelis–Menten-type fitting of the maximum F change ($\Delta F/F_0$) as a function of Ni(II) concentrations ($K_{M,\ Ni(II)} = 26.6 \pm 1.5$ μM and $(\Delta F/F_0)_{MAX} = -0.52 \pm -0.01$ s^{-1}) inset: maximal initial Ni(II) transport rates in NixA proteoliposomes and corresponding fit with a Michaelis–Menten-like equation: $(\delta F/\delta t) = (\delta F/\delta t)_{MAX} \times [Ni(II)]/(K_M + [Ni(II)])$; $K_{M,\ Ni(II)} = 31.0 \pm 1.2$ μM and $(\delta F/\delta t)_{MAX} = -0.0089 \pm -0.0004$ s^{-1}. (D) Fluorescence quenching transport traces upon addition of Ni(II) and Co(II) (25 μM) to NixA proteoliposomes, monitored by FZ-3-Zn(II) probe complex, and Zn(II) transport traces monitored by metal-free FZ-3. Signals were corrected by subtracting the background signal of control liposomes (n = 3). (E) Maximal initial transport rates (initial slope) obtained for control ($-1.22 \pm 0.05 \times 10^{-5}$ s^{-1}), Ni(II) ($-5.51 \pm 0.20 \times 10^{-3}$ s^{-1}), and Co(II) ($-4.35 \pm 0.24 \times 10^{-6}$ s^{-1}) (25 μM) in NixA proteoliposomes monitored by FZ-3-Zn(II) probe, and Zn(II) ($-2.73 \pm 0.20 \times 10^{-5}$) (25 μM) in NixA proteoliposomes using FZ-3. Signals were corrected by subtracting the background signal of control liposomes (n = 3).

fluorescence traces corrected for response of control liposomes, as described for the Ni(II) transport assays. The fluorescence traces ($\Delta F/F_0$) as a function of time, resulting from the NixA-mediated transport, showed a significant exponential quenching response only upon addition of Ni(II), and the absence of signals upon the addition of Co(II) or Zn(II) indicated the lack of translocation activity towards these two substrates. Therefore, this investigation unambiguously confirm that NixA is a high-affinity, Ni(II)-selective Class I NiCoT transporter with low substrate promiscuity (Fig. 2D and E).

Putative Ni(II)/H^+ co-/counter-transport monitored with the pH sensitive probe pyranine

Given the acidic environment (pH 4.5–6.5) of *H. pylori* periplasm, it is hypothesized that NixA could co-transport H^+ while acquiring the metal substrate.[22] To determine if NixA strictly requires and exploit the proton motive force to catalyze Ni(II) translocation, we encapsulated the fluorescent pH sensitive probe pyranine in the proteoliposome lumen. This aryl sulfonate derivative (8-hydroxy-1,3,6-pyrenetrisulfonate) is a water-soluble, membrane-impermeant pH-sensitive probe, with a fluorescent emission centered at 515 nm. The fluorescent emission yield of pyranine depends on the protonation state of the 8-hydroxyl group (pK_a 7.2).[37] These pyranine properties makes it suitable as a membrane-compatible sensor to report pH changes, as it does not bind with the lipid membranes because of the repulsion between negative charges of pyranine and the polar head of the lipids. When pyranine is deprotonated, the increase in pH results in a turn-on fluorescence response. Therefore, encapsulation of pyranine in the liposomal lumen can allow for the monitoring of proton influx or efflux through a decrease or increase in the time-dependent fluorescence signal, respectively.[40] Pyranine was encapsulated in the lumen of control liposomes and NixA proteoliposomes by freeze–thaw membrane fracture. Ni(II) transport was triggered by rapid mixing with buffered solutions containing Ni(II), and the fluorescence traces were recorded at the pyranine emission maxima (λ_{exc} = 480 nm: λ_{em} = 515 nm), utilizing identical time frames used to study Ni(II) transport with the FZ-3-Zn(II) probe. Analysis of the kinetic traces revealed no detectable change in pyranine fluorescence in NixA proteoliposomes, with identical traces compared to control liposomes. This analysis indicates that, under the condition used, no H^+ transport occurs upon Ni(II) translocation (Fig. 3A). Thus, the presence of a proton motive force is not a strict requirement for NixA-mediated Ni(II) translocation, even though the role of the proton gradient in promoting Ni(II) acquisition *in vivo* remains to be investigated in detail. Regardless, our observation reveals a novel mechanistic feature of NixA translocation, as no NiCoT permease has been characterized using pyranine in previous studies.

Electrogenic Ni(II) transport monitored by the membrane potential probe oxonol VI

The results from the metal transport assays with FZ-3-Zn(II) and H^+ proton translocation with pyranine revealed that NixA potentially allows the selective translocation of Ni(II) across without a net proton co-/counter-transport. Therefore, we postulated that Ni(II) translocation by NixA could be electrogenic, resulting in the accumulation of net positive charges in the proteoliposomes, if no other ion (*e.g.* Na^+) is co-transported.

In order to determine Ni(II) transport electrogenicity, oxonol VI (bis-(3-propyl-5-oxoisoxazol-4-yl) pentamethine oxonol) was used as a probe to monitor the changes in transmembrane membrane potential (Ψ). Oxonols are known to be relatively slow-response fluorescent probes that detects transmembrane membrane potential by differential partitioning between the aqueous phase and lipid bilayers. This change in partitioning as a function of membrane potential results in a modification of the fluorescence response. Compared to other oxonol compounds, oxonol VI has the fastest response to changes in potential.[38,41] These characteristics make oxonol VI suitable for the real-time monitoring of transmembrane potential in liposomes and in cells, allowing the study of ion channels and electrogenic pumps.[38,41]

To test if the transport of Ni(II) is electrogenic, the same methodologies were employed for oxonol VI reconstitution in NixA proteoliposomes, as described for the metal transport assays. The fluorescence kinetic traces were analyzed at the oxonol VI emission maximum (λ_{exc} = 580 nm: λ_{em} = 660 nm), upon mixing the proteoliposomes with Ni(II) stock solutions to trigger substrate translocation. Analysis of the fluorescence kinetic traces indicated that, as Ni(II) is translocated by NixA inside the proteoliposome lumen, a transmembrane potential is generated as a result of an accumulation of net positive charges, resulting in an increase in the oxonol VI fluorescence response. Thus, at least under the condition used, the transport the NixA-mediated Ni(II) transport is electrogenic, creating a net transfer of positive charges from the extravesicular environment into the proteoliposome lumen.

To further substantiate that the positive-inside membrane potential generated in the proteoliposome lumen (detected by oxonol VI) is a result of Ni(II) transport (as monitored by FZ-3-Zn(II)), we normalized the signals obtained from these transport assays and overlapped their kinetic traces. The almost perfect superimposition of the traces confirms that the net translocation of the positive charges stems from the translocation of Ni(II) (Fig. 3B). Together, this analysis also substantiates that the Ni(II) translocation monitored by FZ-3-Zn(II) reports the metal translocation events in real-time.

In conclusion, our developed platform based on fluorescent reporter probes sensitive to different stimuli (metal substrates, pH, transmembrane potential) provides a new tool to study the translocation properties and mechanism of NixA, and could potentially be applied to other Ni(II) transporters. Based on the analysis, we discovered that *H. pylori* NixA is a non-promiscuous transmembrane electrogenic uniporter strictly selective for Ni(II).

Mutation studies of NixA Ni(II) translocation pathway

Topology prediction of NixA analyzed with TOPCONS, indicated that the protein contains eight transmembrane (TM) helices with a long hydrophilic loop connecting TM IV and TM V.[21] Previous *in vivo* studies have shown that important conserved motifs (also known as recognition sequences), potentially responsible for substrate recognition and translocation, are present in TM II and TM III. These conserved motifs in TM II and TM III are (HA(F/V)DADH(I/L)) and $(G(Xaa)_5GHSSVV)$, respectively.[21,23] As we developed a methodology to monitor the transport properties of purified NixA reconstituted in proteoliposomes, we proceeded to further dissect the critical residues responsible for substrate recognition and transport *via* mutation studies. We introduced selected single and combination mutations in NixA based on *in vivo* studies which analyzed

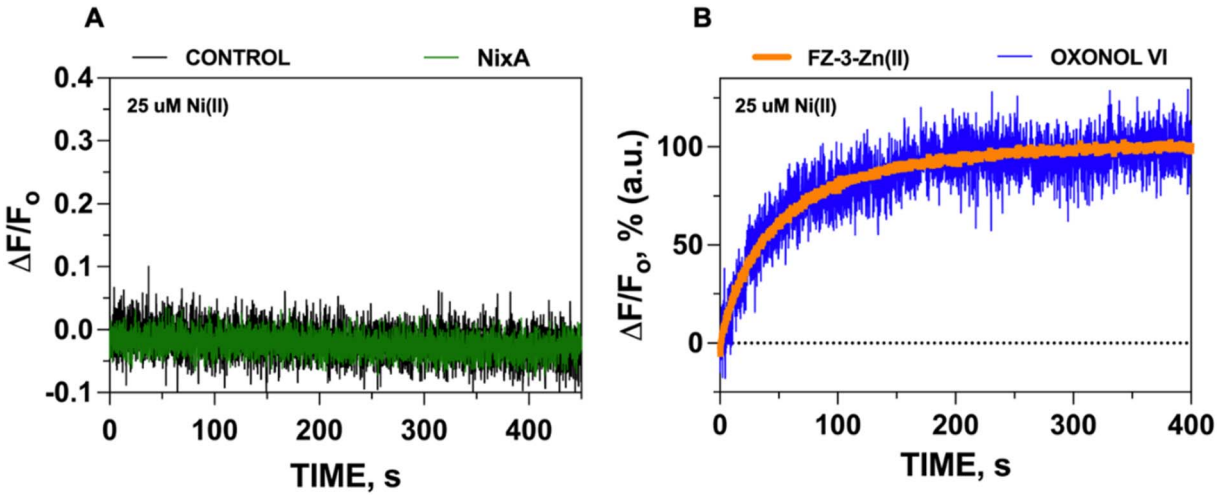

Fig. 3 Determination of H^+ transport and electrogenicity in NixA proteoliposomes. (A) Determination of H^+ translocation in NixA proteoliposomes upon Ni(II) transport (Ni(II) = 25 μM) monitored by tracking changes in luminal pH as a function of time, utilizing the pH indicator pyranine (n = 3). (B) Superimposition of kinetic traces of Ni(II) transport monitored by FZ-3-Zn(II) and transmembrane potential changes monitored by oxonol VI. The kinetic traces were normalized and corrected with corresponding the control background signals (n = 3). The close correspondence of the two traces are consistent with a positive-inside transmembrane potential generated by NixA-mediated Ni(II) transport.

membrane extracts and quantified the protein activity through cellular metal accumulation assays and urease activity.[21,29,30,32] The structural model of NixA (*H. pylori*) generated by AlphaFold as previously described (Fig. 4A)[11] was used to identify and locate the relative positions of the amino acids in these recognition sequences. Based on the model, the NixA conserved motifs (HA(F/V)DADH(I/L) and G(Xaa)$_5$GHSSVV) were located in the innermost part of the transmembrane protein scaffold that spans from the periplasm to the cytoplasm (Fig. 4B).[30,32] *In vivo* studies identified that mutations in TM II (H44I, D47I, D49I, H50I, D55I), TM III (H79I) and TM VI (D23I, D234I) caused reduced metal accumulation and/or reduced/abolished urease activity.[30] We assessed the relative positions of these conserved amino acid sequences in the structural model and noticed that these residues were arranged in a transmembrane pathway-like structure which consisted of an entry point, translocation core, and exit point (Fig. 4B).

Five NixA combination mutants were initially designed, based on potential metal-coordinating amino acid residues clustered in each position in the translocation pathway, which were replaced with a non-coordinating alanine (Table 1). These mutant proteins were expressed, purified in stable forms (ESI Fig. S4†), and reconstituted utilizing the same protocols described for wild-type NixA. After purification, the monodisperse proteins were successfully incorporated into proteoliposomes with the same reconstitution efficiencies as compared to wild-type NixA (Fig. 5A), and the effect of the mutations in the transport activity – whether they changed the substrate recognition and/or terminated the protein activity – were investigated. The transport assays of these mutants were carried out as described for wtNixA. Analysis of the transport traces and their respective apparent initial transport velocities revealed that the Ni(II) transport activities of all these combination mutants were completely abolished, substantiating key roles of these residues in the NixA transmembrane translocation pathway (Fig. 5B, ESI S5, and Table S2†).

To further understand the role of each combination mutations in recognition and Ni(II) binding, we performed metal-binding determinations. Samples were prepared by mixing the purified NixA and mutants in detergent micelles with metal substrate in a 1 : 3 molar ratio; then, weakly bound and unbound metals were removed by SEC. Protein concentrations were determined *via* a modified Bradford assays, and Ni(II) concentrations were determined by ICP-MS. Analysis of the Ni(II) stoichiometry ratios revealed that wtNixA features two high-affinity transmembrane metal binding sites (Ni(II):NixA = 2.0 ± 0.3 ion mol^{-1}; Fig. 5C).

To estimate the binding affinity of these two Ni(II) binding sites, Isothermal Titration Calorimetry (ITC) determinations were conducted on wtNixA samples. Ni(II) titration of NixA produced an exothermic reaction, as indicated by negative peaks following each injection of Ni(II), with a biphasic behavior, revealing the presence of two distinct binding events. This observation, together with the results of the metal analysis discussed above, clearly hints to the presence of two binding sites on wtNixA, each containing a single Ni(II) ion (Fig. 5D, upper panel). The integrated heat data were fitted using either a stoichiometric equilibria (SE) model or an independent sites (IS) model (both assuming two sets of single-metal-binding sites) (Fig. 5D, lower panel). The goodness-of-fit parameters obtained for the two models are identical (see ESI Table 3† for a complete list of the fitted parameters), so that a clear distinction cannot be made. The detailed speciation and heat contribution to the binding isotherms for the fits of the two models are provided in ESI Fig. S6–S9.†

The dissociation constants are in the low μM range for both models (K_{D1} (SE) = 1.3 ± 0.4 μM, K_{D1} (IS) = 1.6 ± 0.4 μM, and K_{D2} (SE) = 9.2 ± 3.9 μM, K_{D2} (IS) = 7.7 ± 2.4 μM), confirming the

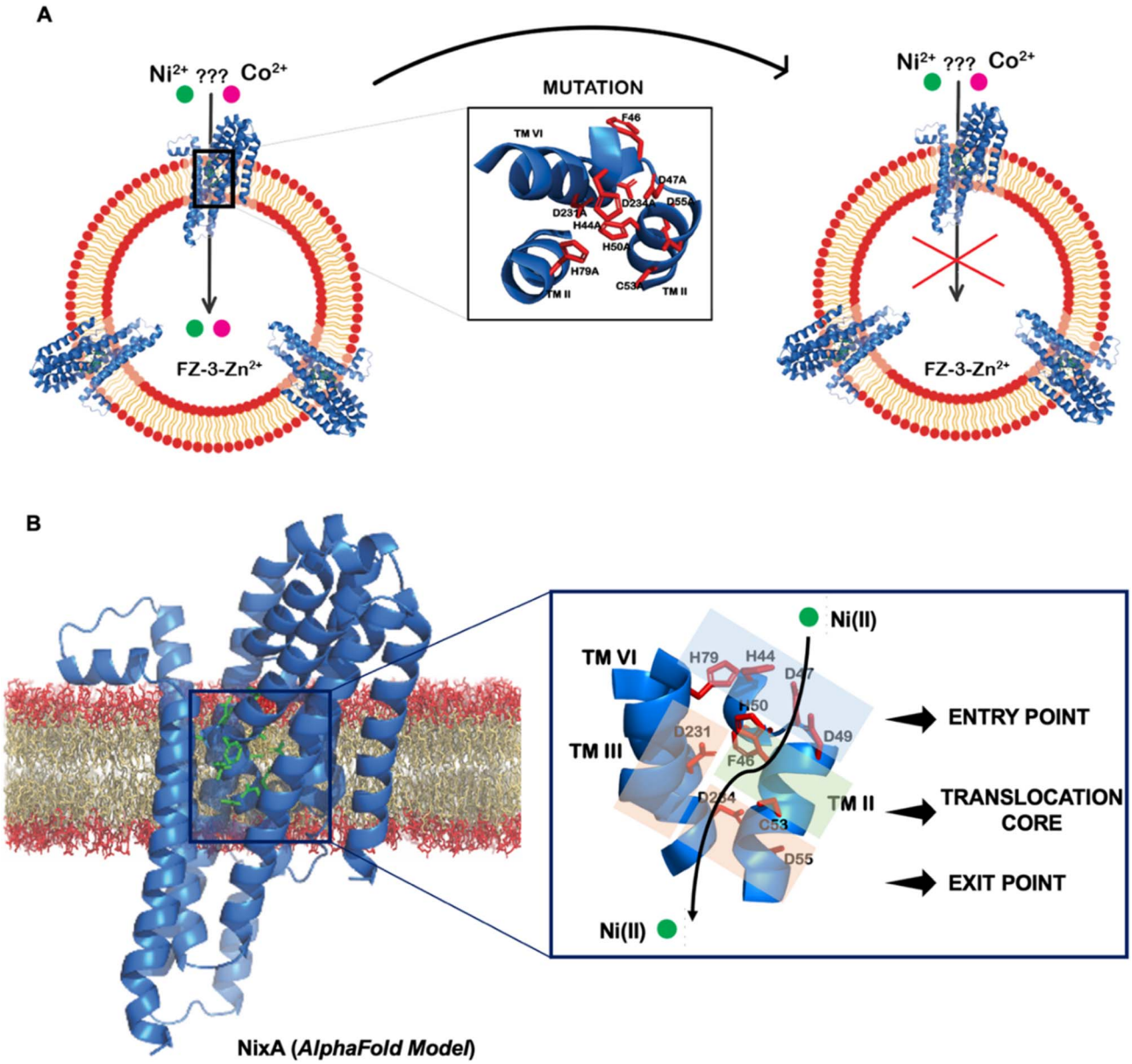

Fig. 4 Structural model of NixA (*H. pylori*). (A) Schematic depicting the AlphaFold model for NixA and approach to study key transmembrane residues essential for transport activity. (B) Relative position of conserved NiCoT permeases recognition motifs and the putative translocation pathway based on the AlphaFold model.

characteristic of tight binding for both sites. The estimated sub-stoichiometric active protein concentration (r_M *ca.* 44% for both models) might result from residual metal copurification in the proteins samples (approx. 15%, as determined by ICP-OES), together with a potential equilibrium with one or multiple conformational states inaccessible to metal binding, and/or partial loss of protein activity due to sample partial aggregation or degradation. Nevertheless, in agreement with the presence of two distinct binding sites in NixA, the two binding events showed different thermodynamic properties. The first binding event is both enthalpically and entropically driven (ESI Table S3†), while the second binding event is enthalpically driven while possessing a negative entropic contribution (ESI Table S3†).

While the stoichiometry of Ni(II) binding to D231A/D234A NixA (1.5 ± 0.4 mol mol^{-1}) and D47A/D231A/D234A NixA (1.8 ± 0.6 mol mol^{-1}) was not drastically affected, the two mutants H44A/D47A/H79A and H44A/D47A/D49A showed completely abolished Ni(II) binding abilities. Contrarily, the D49A/H50A/D55A mutant showed decreased binding (1.2 ± 0.2 mol mol^{-1}) consistent with the alteration on only one of the two high affinity binding sites (Fig. 5C). Based on this analysis, and consistent with the AlphaFold structural model, we conclude that the amino acid residues H44, D47, D49, H79, which are situated in the entry point of the translocation pathway, are centrally involved not only in translocation but also in the first step of metal recognition and binding.

Table 1 NixA mutants and relative positions of the mutations based on the AlphaFold model

Mutant name	Transmembrane helix	Amino acid mutations	Position in the translocation pathway
H44A_D47A_H79A	TM2	H44A	Entry point
		D47A	
	TM3	H79A	
H44A_D47A_D49A	TM2	H44A	Entry point
		D47A	
		D49A	
D49A_D50A_D55A	TM2	D49A	Translocation core
		H50A	
		D55A	
D231A_D234A	TM6	D231A	Translocation core
		D234A	
D47A_D231A_D234A	TM2	D47A	Exit point
	TM6	D231A	
		D234A	

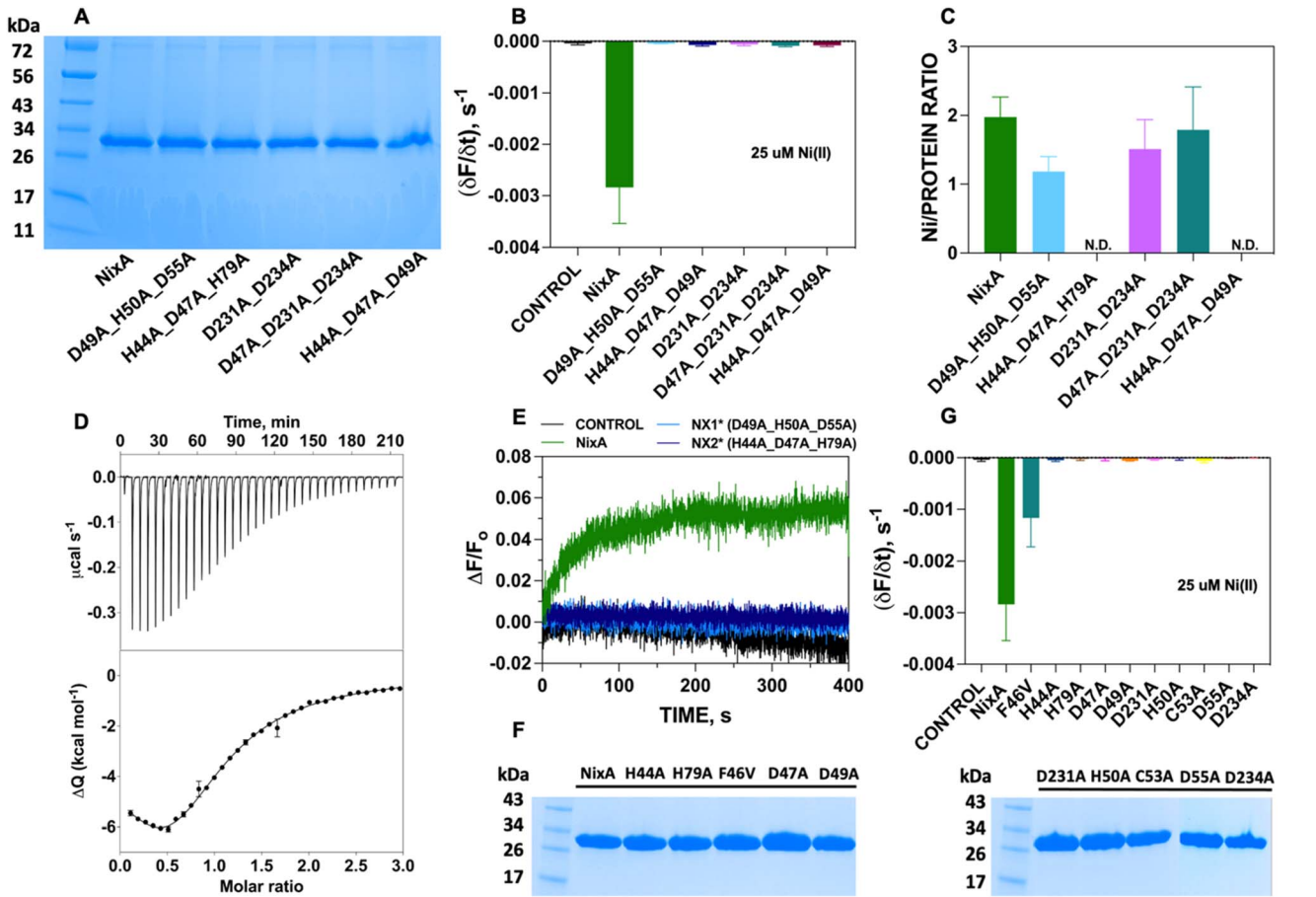

Fig. 5 NixA mutation studies. (A) SDS-PAGE analysis of NixA and NixA combination mutants reconstituted in proteoliposomes utilized for the Ni(II) transport assays. (B) Maximal initial Ni(II) transport rates by NixA and combination mutants monitored in proteoliposomes with FZ-3-Zn(II) encapsulated in the SUV lumen (25 μM; $\lambda_{exc} = 480$ nm; $\lambda_{em} = 515$ nm) ($n = 3$). (C) NixA and NixA mutants Ni(II) binding stoichiometry measured by ICP-MS (Ni(II) concentration) and Bradford assays (protein concentration) ($n = 3$). (D) Ni(II) titration of HpNixA followed by ITC. Heat response for injections of 400 μM Ni(II) into 20 μM HpNixA (top); integrated heat data of the titration as a function of Ni(II)/NixA molar ratio. The continuous line represents the best fit (goodness of fit, GoF = 78.4%) obtained with a stoichiometric equilibria model which involves two sets of metal-binding sites (bottom). (E) Real-time traces of transmembrane potential generation by NixA, NX1, and NX2 mutants in proteoliposomes upon incubation with Ni(II) (25 μM), monitored by encapsulating oxonol VI in the proteoliposome lumen ($n = 3$). (F) SDS-PAGE analysis of NixA and single-point NixA mutants reconstituted in proteoliposomes utilized for Ni(II) transport assays. (G) Maximal initial Ni(II) transport rates in NixA and NixA point-mutants monitored in proteoliposomes with FZ-3-Zn(II) encapsulated in the SUV lumen (Ni(II) = 25 μM; $\lambda_{exc} = 480$ nm; $\lambda_{em} = 515$ nm) ($n = 3$).

To further support and validate our findings, we performed oxonol VI experiments on two representative mutants: D49A/H50A/D55A (capable of binding one Ni(II) instead of two, with no transport) and H44A/D47A/H79A (incapable of Ni(II) binding, with no transport). The working hypothesis were as follows: if these mutants eliminated the ability of NixA to bind and/or transport Ni(II), no response from oxonol VI should be observed, as no Ni(II) substrate can be bound and/or transported. Kinetic traces from the oxonol VI electrogenicity assay showed complete absence of turn-on fluorescence signal, indicating that no electrogenic Ni(II) transport occurred upon mutation of these key residues (Fig. 5E).

Given the results obtained on the combination mutants, single-point mutants in the translocation pathway were generated to further identify and dissect the contribution of each amino acid residue to NixA transport activity. These mutants were expressed, purified (ESI Fig. 4†), and reconstituted into liposomes. The SDS-PAGE analysis of the corresponding proteoliposomes pellets showed identical incorporation efficiency in proteoliposomes as observed for wtNixA (Fig. 5F). Transport assays on proteoliposomes in the presence of Ni(II), monitored by FZ-3-Zn(II), were conducted as described for the wtNixA to determine the relative transport activity of each mutant. Transport traces collected on H44A, H79A, D47A, D49A, H50A, C53A, D55A, D231A, and D234A NixA single-site mutants showed absence of quenching response, indicating the total abolishment of Ni(II) transport activity, with the exception of F46V which displayed reduced transport activity compared to NixA (~33%, Fig. 5G, ESI 5, and Table S2†). The amino acid (F/V) in the conserved motif at TM II (HAF/VDADHIA) in NiCoTs has been postulated to be potentially responsible for the selectivity towards Ni(II) *vs.* Co(II) substrates.[21] Our data suggest that phenylalanine indeed contributes, but is not critical, for the transport of Ni(II). The role of this phenylalanine in modulating substrate selectivity can potentially arise from putative cation–π interactions in the selectivity filter.

Based on this data, we can conclude that H44, H79, D47, D49, H50, C53, D55, D231, and D234 are critical residues in Ni(II) translocation by NixA, further supporting the structural model which indicate the presence of a three-stage translocation pathway. These findings, moreover, validate *in vivo* observations on some of these mutants investigated *via* Ni(II) accumulation assays or urease activation.[21,29,30,32] Overall, our work further supports that NixA evolved chemically and structurally to exclusively recognize and transport Ni(II), owing to the presence of a characteristic transmembrane recognition and translocation pathway characterized by an arrangement of key and conserved metal coordinating residues which allow non-promiscuous Ni(II) substrate recognition and transport.

Conclusions

In summary, this work established a platform to recombinantly express and purify transmembrane NiCoT transporter proteins in active form, which allowed us to reconstitute them in artificial lipid bilayer vesicles to study Ni(II) translocation events, transport mechanism, and kinetics. This study also revealed that *H. pylori* NixA is a Class I NiCoT permease with no substrate promiscuity. The transport assays in proteoliposomes substantiate that NixA is a high affinity, high-capacity Ni(II) transporter with $K_{M,\ Ni(II)} = 31.0 \pm 1.2$ μM, allowing for the uptake of Ni(II) at physiologically relevant concentrations with fast translocation rates. Unprecedented co-transport and electrogenicity measurements in proteoliposomes carrying a purified NiCoT transporter revealed that NixA can act as an electrogenic Ni(II) uniporter. Mutational analysis identified key transmembrane residues (H44, D47, H79, and D49) that are critical in high-affinity Ni(II) binding, which together with a number of additional transmembrane (possibly transient) coordinating residues (H50, C53, D55, D231, and D234) create a potential three-stage transmembrane translocation pathway to allow for the selective translocation of Ni(II) across the lipid bilayer. A detail comparison of NixA transport properties with the other Ni(II) importer present in *H. pylori*, the Ni(II) ABC transporter NiuBDE, is limited by the lack of detailed molecular-level structural and functional characterizations of the transmembrane component of Ni(II) ABC transporter systems. While the NikABCDE protein complex found in the *E. coli* inner membrane is the canonical and best characterized nickel-responsive ABC transporter, only its periplasmic substrate binding protein (SBP), NikA, is well-characterized. Apo- and holo- NikA crystal structures featuring a classical SBP topology and coordination of one Ni(II) ion (with aquo or L-histidine ligands) have been reported, and a Ni(II) dissociation constant (K_D) of approx. 10 μM has been determined by ITC, showing a similar affinity regime as determined for NixA in this study.[42,43] Studies on NikA homologues have suggested that NikA and other Ni-SBPs are highly promiscuous, binding to different nickel forms (complexes) during uptake.[42–44] However, the Ni(II) affinities and transport kinetics of the transmembrane transporter component, responsible for transmembrane Ni(II) translocation across the lipid bilayer, remain to be established. Thus, this study, carried out for the first time on NixA, opens new venues to investigate and understand the transport properties of other NiCoT transporter subclasses as well as other Ni(II) transporter families, which will allow for a detailed comparative investigations of their diverse Ni(II) translocation properties.

Data availability

Data for this paper are available upon request to the corresponding author.

Author contributions

Jayoh A. Hernandez: investigation, formal analysis, methodology, writing – original draft; Paul S. Micus, Sean Alec Lois Sunga: investigation, formal analysis, methodology, writing – review & editing; Luca Mazzei, Stefano Ciurli: investigation, formal analysis, methodology, writing, resources; Gabriele Meloni: conceptualization, supervision, investigation, formal analysis, methodology, writing – original draft, resources.

Conflicts of interest

The authors declare no conflict of interest.

Acknowledgements

The work was supported by the National Institute of General Medical Sciences of the National Institutes of Health under Award Number R35GM128704 (to G. M.) and by the Robert A. Welch Foundation (AT-2073-20210327 to G. M). The content is solely the responsibility of the authors and does not necessarily represent the official views of the National Institutes of Health. L. M. and S. C. received financial support from the University of Bologna and the Consorzio Interuniversitario di Risonanze Magnetiche di Metallo-Proteine (CIRMMP).

References

1 H. B. Gray, E. I. Stiefel, J. S. Valentine, and I. Bertini, *Biological Inorganic Chemistry Structure and Reactivity*, University Science Books, Sausalito, Californie, 1st edn, 2007.
2 L. D. Palmer and E. P. Skaar, Transition Metals and Virulence in Bacteria, *Annu. Rev. Genet.*, 2016, **50**, 67–91.
3 M. J. Maroney and S. Ciurli, Nonredox nickel enzymes, *Chem. Rev.*, 2014, **114**, 4206–4228.
4 M. J. Maroney and S. Ciurli, Nickel as a virulence factor in the Class I bacterial carcinogen, Helicobacter pylori, *Semin. Cancer Biol.*, 2021, **76**, 143–155.
5 M. R. Leach and D. B. Zamble, Metallocenter assembly of the hydrogenase enzymes, *Curr. Opin. Chem. Biol.*, 2007, **11**, 159–165.
6 Y. Li and D. B. Zamble, Nickel homeostasis and nickel regulation: an overview, *Chem. Rev.*, 2009, **109**, 4617–4643.
7 H. Kaluarachchi, K. C. Chan Chung and D. B. Zamble, Microbial nickel proteins, *Nat. Prod. Rep.*, 2010, **27**, 681–694.
8 A. M. Sydor and D. B. Zamble, Nickel metallomics: general themes guiding nickel homeostasis, *Met. Ions Life Sci.*, 2013, **12**, 375–416.
9 C. J. Zeer-Wanklyn and D. B. Zamble, Microbial nickel: cellular uptake and delivery to enzyme centers, *Curr. Opin. Chem. Biol.*, 2017, **37**, 80–88.
10 T. Eitinger and M. A. Mandrand-Berthelot, Nickel transport systems in microorganisms, *Arch. Microbiol.*, 2000, **173**, 1–9.
11 G. Camporesi, A. Minzoni, L. Morasso, S. Ciurli and F. Musiani, Nickel import and export in the human pathogen Helicobacter pylori, perspectives from molecular modelling, *Metallomics*, 2021, **13**(12), mfab066.
12 F. Musiani, B. Zambelli, M. Bazzani, L. Mazzei and S. Ciurli, Nickel-responsive transcriptional regulators, *Metallomics*, 2015, **7**, 1305–1318.
13 P. Ruggiero, Helicobacter pylori and inflammation, *Curr. Pharm. Des.*, 2010, **16**, 4225–4236.
14 L. Mazzei, F. Musiani and S. Ciurli, The structure-based reaction mechanism of urease, a nickel dependent enzyme: tale of a long debate, *J. Biol. Inorg. Chem.*, 2020, **25**, 829–845.
15 S. B. Mulrooney and R. P. Hausinger, Nickel uptake and utilization by microorganisms, *FEMS Microbiol. Rev.*, 2003, **27**, 239–261.
16 M. I. Hood and E. P. Skaar, Nutritional immunity: transition metals at the pathogen-host interface, *Nat. Rev. Microbiol.*, 2012, **10**, 525–537.
17 F. Fischer, M. Robbe-Saule, E. Turlin, F. Mancuso, V. Michel, P. Richaud, F. J. Veyrier, H. De Reuse and D. Vinella, Characterization in Helicobacter pylori of a Nickel Transporter Essential for Colonization That Was Acquired during Evolution by Gastric Helicobacter Species, *PLoS Pathog.*, 2016, **12**, e1006018.
18 D. A. Rodionov, P. Hebbeln, M. S. Gelfand and T. Eitinger, Comparative and functional genomic analysis of prokaryotic nickel and cobalt uptake transporters: evidence for a novel group of ATP-binding cassette transporters, *J. Bacteriol.*, 2006, **188**, 317–327.
19 T. Eitinger, J. Suhr, L. Moore and J. A. C. Smith, Secondary transporters for nickel and cobalt ions: theme and variations, *BioMetals*, 2005, **18**, 399–405.
20 P. Hebbeln and T. Eitinger, Heterologous production and characterization of bacterial nickel/cobalt permeases, *Fems Microbiol. Lett.*, 2004, **230**, 129–135.
21 O. Degen and T. Eitinger, Substrate specificity of nickel/cobalt permeases: Insights from mutants altered in transmembrane domains I and II, *J. Bacteriol.*, 2002, **184**, 3569–3577.
22 O. Degen, M. Kobayashi, S. Shimizu and T. Eitinger, Selective transport of divalent cations by transition metal permeases: the Alcaligenes eutrophus HoxN and the Rhodococcus rhodochrous NhlF, *Arch. Microbiol.*, 1999, **171**, 139–145.
23 T. Eitinger, L. Wolfram, O. Degen and C. Anthon, A Ni^{2+} binding motif is the basis of high affinity transport of the Alcaligenes eutrophus nickel permease, *J. Biol. Chem.*, 1997, **272**, 17139–17144.
24 T. Eitinger and B. Friedrich, A Topological Model for the High-Affinity Nickel Transporter of Alcaligenes Eutrophus, *Mol. Microbiol.*, 1994, **12**, 1025–1032.
25 T. Eitinger and B. Friedrich, Cloning, Nucleotide-Sequence, and Heterologous Expression of a High-Affinity Nickel Transport Gene from Alcaligenes-Eutrophus, *J. Biol. Chem.*, 1991, **266**, 3222–3227.
26 N. Noinaj, M. Guillier, T. J. Barnard and S. K. Buchanan, TonB-dependent transporters: regulation, structure, and function, *Annu. Rev. Microbiol.*, 2010, **64**, 43–60.
27 A. H. van Vliet, J. Stoof, R. Vlasblom, S. A. Wainwright, N. J. Hughes, D. J. Kelly, S. Bereswill, J. J. Bijlsma, T. Hoogenboezem, C. M. Vandenbroucke-Grauls, M. Kist, E. J. Kuipers and J. G. Kusters, The role of the Ferric Uptake Regulator (Fur) in regulation of Helicobacter pylori iron uptake, *Helicobacter*, 2002, **7**, 237–244.
28 K. Postle, TonB system, in vivo assays and characterization, *Methods Enzymol.*, 2007, **422**, 245–269.
29 J. F. Fulkerson Jr and H. L. Mobley, Membrane topology of the NixA nickel transporter of Helicobacter pylori: two nickel transport-specific motifs within transmembrane helices II and III, *J. Bacteriol.*, 2000, **182**, 1722–1730.

30 J. F. Fulkerson Jr, R. M. Garner and H. L. Mobley, Conserved residues and motifs in the NixA protein of Helicobacter pylori are critical for the high affinity transport of nickel ions, *J. Biol. Chem.*, 1998, **273**, 235–241.

31 X. Deng, J. M. He and N. He, Comparative study on Ni^{2+}-affinity transport of nickel/cobalt permeases (NiCoTs) and the potential of recombinant Escherichia coli for Ni^{2+} bioaccumulation, *Bioresour. Technol.*, 2013, **130**, 69–74.

32 L. Wolfram and P. Bauerfeind, Conserved low-affinity nickel-binding amino acids are essential for the function of the nickel permease NixA of Helicobacter pylori, *J. Bacteriol.*, 2002, **184**, 1438–1443.

33 K. R. Gee, Z. L. Zhou, W. J. Qian and R. Kennedy, Detection and imaging of zinc secretion from pancreatic beta-cells using a new fluorescent zinc indicator, *J. Am. Chem. Soc.*, 2002, **124**, 776–778.

34 J. Zhao, B. A. Bertoglio, M. J. Devinney Jr, K. E. Dineley and A. R. Kay, The interaction of biological and noxious transition metals with the zinc probes FluoZin-3 and Newport Green, *Anal. Biochem.*, 2009, **384**, 34–41.

35 S. S. Abeyrathna, N. S. Abeyrathna, N. K. Thai, P. Sarkar, S. D'Arcy and G. Meloni, IroT/MavN Is a Legionella Transmembrane Fe(II) Transporter: Metal Selectivity and Translocation Kinetics Revealed by in Vitro Real-Time Transport, *Biochemistry*, 2019, **58**, 4337–4342.

36 S. S. Abeyrathna, N. S. Abeyrathna, P. Basak, G. W. Irvine, L. Zhang and G. Meloni, Plastic recognition and electrogenic uniport translocation of 1^{st}-, 2^{nd}-, and 3^{rd}-row transition and post-transition metals by primary-active transmembrane $P_{1B\text{-}2}$-type ATPase pumps, *Chem. Sci.*, 2023, **14**, 6059–6078.

37 N. R. Clement and J. M. Gould, Pyranine (8-hydroxy-1,3,6-pyrenetrisulfonate) as a probe of internal aqueous hydrogen ion concentration in phospholipid vesicles, *Biochemistry*, 1981, **20**, 1534–1538.

38 H. J. Apell and B. Bersch, Oxonol VI as an optical indicator for membrane potentials in lipid vesicles, *Biochim. Biophys. Acta*, 1987, **903**, 480–494.

39 A. Pineiro, E. Munoz, J. Sabin, M. Costas, M. Bastos, A. Velazquez-Campoy, P. F. Garrido, P. Dumas, E. Ennifar, L. Garcia-Rio, J. Rial, D. Perez, P. Fraga, A. Rodriguez and C. Cotelo, AFFINImeter: A software to analyze molecular recognition processes from experimental data, *Anal. Biochem.*, 2019, **577**, 117–134.

40 K. Wang, O. Sitsel, G. Meloni, H. E. Autzen, M. Andersson, T. Klymchuk, A. M. Nielsen, D. C. Rees, P. Nissen and P. Gourdon, Structure and mechanism of Zn^{2+}-transporting P-type ATPases, *Nature*, 2014, **514**, 518–522.

41 R. J. Clarke and H. J. Apell, A stopped-flow kinetic study of the interaction of potential-sensitive oxonol dyes with lipid vesicles, *Biophys. Chem.*, 1989, **34**, 225–237.

42 J. Heddle, D. J. Scott, S. Unzai, S. Y. Park and J. R. H. Tame, Crystal Structures of the Liganded and Unliganded Nickel-Binding Protein NikA from Escherichia Coli, *J. Biol. Chem.*, 2003, **278**, 50322–50329.

43 H. Lebrette, M. Iannello, J. C. Fontecilla-Camps and C. Cavazza, The Binding Mode of Ni-$(L\text{-}His)_2$ in NikA Revealed by X-Ray Crystallography, *J. Inorg. Biochem.*, 2013, **121**, 16–18.

44 H. Lebrette, C. Brochier-armanet, B. Zambelli, H. de Reuse, E. Borezée-Durant, S. Ciurli and C. Cavazza, Promiscuous Nickel Import in Human Pathogens: Structure, Thermodynamics, and Evolution of Extracytoplasmic Nickel-Binding Proteins, *Structure*, 2014, **22**, 1421–1432.